

AD-R167 598

ANALYSIS OF DICKE NARROWING IN WALL-COATED AND
BUFFER-GAS-FILLED ATOMIC S. (U) AEROSPACE CORP EL
SEQUONDO CA CHEMISTRY AND PHYSICS LAB

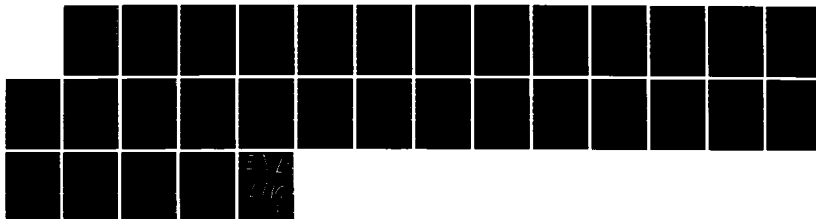
1/1

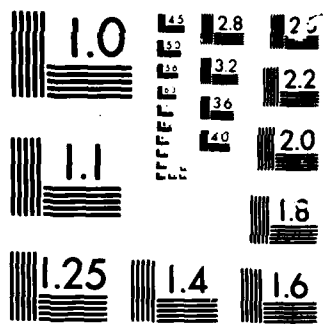
UNCLASSIFIED

R P FRUEHOLZ ET AL. 81 APR 86

F/G 7/4

NL





MICROCOR

CHART

AD-A167 598

REPORT SD-TR-86-13

(12)

Analysis of Dicke Narrowing in Wall-Coated and Buffer-Gas-Filled Atomic Storage Cells

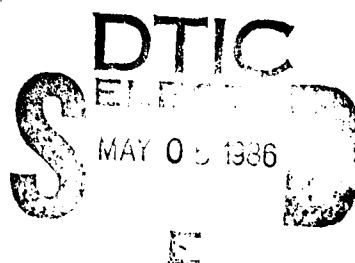
R. P. FRUEHOLZ
Chemistry and Physics Laboratory
Laboratory Operations
The Aerospace Corporation
El Segundo, CA 90245

and

C. H. VOLK
Litton Industries
Guidance and Control Systems
Woodland Hills, CA 91367

1 April 1986

APPROVED FOR PUBLIC RELEASE;
DISTRIBUTION UNLIMITED



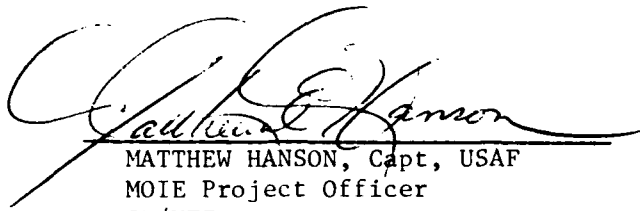
FILE COPY
FILE COPY
FILE COPY

Prepared for
SPACE DIVISION
AIR FORCE SYSTEMS COMMAND
Los Angeles Air Force Station
P.O. Box 92960, Worldway Postal Center
Los Angeles, CA 90009-2960

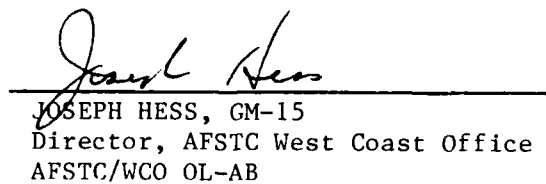
This report was submitted by The Aerospace Corporation, El Segundo, CA 90245, under Contract No. F04701-85-C-0086 with the Space Division, P.O. Box 92960, Worldway Postal Center, Los Angeles, CA 90009-2960. It was reviewed and approved for The Aerospace Corporation by S. Feuerstein, Director, Chemistry and Physics Laboratory. Capt. Matthew Hanson, SD/YEZ, was the project officer for the Mission-Oriented Investigation and Experimentation (MOIE) program.

This report has been reviewed by the Public Affairs Office (PAS) and is releasable to the National Technical Information Service (NTIS). At NTIS, it will be available to the general public, including foreign nationals.

This technical report has been reviewed and is approved for publication. Publication of this report does not constitute Air Force approval of the report's findings or conclusions. It is published only for the exchange and stimulation of ideas.



MATTHEW HANSON, Capt, USAF
MOIE Project Officer
SD/YEZ



JOSEPH HESS, GM-15
Director, AFSTC West Coast Office
AFSTC/WCO OL-AB

UNCLASSIFIED

SECURITY CLASSIFICATION OF THIS PAGE (When Data Entered)

REPORT DOCUMENTATION PAGE		READ INSTRUCTIONS BEFORE COMPLETING FORM
1. REPORT NUMBER SD-TR-86-13	2. GOVT ACCESSION NO. ADA 167598	3. RECIPIENT'S CATALOG NUMBER
4. TITLE (and Subtitle) Analysis of Dicke Narrowing in Wall-Coated and Buffer-Gas-Filled Atomic Storage Cells		5. TYPE OF REPORT & PERIOD COVERED
		6. PERFORMING ORG. REPORT NUMBER TR-0086(6945-05)-1
7. AUTHOR(s) R. P. Frueholz and C. H. Volk		8. CONTRACT OR GRANT NUMBER(s) F04701-85-C-0086
9. PERFORMING ORGANIZATION NAME AND ADDRESS The Aerospace Corporation El Segundo, CA 90245		10. PROGRAM ELEMENT, PROJECT, TASK AREA & WORK UNIT NUMBERS
11. CONTROLLING OFFICE NAME AND ADDRESS Space Division Los Angeles Air Force Station Los Angeles, CA 90009-2960		12. REPORT DATE 1 April 1986
		13. NUMBER OF PAGES 25
14. MONITORING AGENCY NAME & ADDRESS (if different from Controlling Office)		15. SECURITY CLASS. (of this report) Unclassified
		15a. DECLASSIFICATION/DOWNGRADING SCHEDULE
16. DISTRIBUTION STATEMENT (of this Report) Approved for public release; distribution unlimited.		
17. DISTRIBUTION STATEMENT (of the abstract entered in Block 20, if different from Report)		
18. SUPPLEMENTARY NOTES		
19. KEY WORDS (Continue on reverse side if necessary and identify by block number) Atomic clocks Hyperfine lineshapes Motional narrowing		
20. ABSTRACT (Continue on reverse side if necessary and identify by block number) Spectral lineshape narrowing of atomic vapor emission in a bufferless, wall-coated absorption cell--Dicke narrowing--has been analyzed using the same formalism developed to describe sub-Doppler linewidths in a buffered cell. Within this formalism, lineshapes are generated using Monte Carlo techniques. Linewidth reductions occur in the bufferless cell that are much greater than those in the buffered cell, because of the high probability that Doppler shifts before and after a particular wall collision will cancel each other.		

UNCLASSIFIED

SECURITY CLASSIFICATION OF THIS PAGE(When Data Entered)

19. KEY WORDS (Continued)

20. ABSTRACT (Continued)

The formalism described allows more physical insight than the classic one-dimensional box model previously invoked to explain spectral narrowing in bufferless, wall-coated cells. Additionally, this formalism reveals a correlation between postcollision velocities and intercollision times in the buffered cell, resulting in modifications of the standard Dicke analysis of these cells.

Keywords : Time clocks; motional narrowing,

UNCLASSIFIED

SECURITY CLASSIFICATION OF THIS PAGE(When Data Entered)

CONTENTS

1. INTRODUCTION.....	5
2. ANALYSIS AND RESULTS.....	11
2.1 Analysis of Motional Narrowing in the Wall-Coated Cell.....	12
2.2 Analysis of Motional Narrowing in the Buffer-Gas Case.....	18
2.3 Discussion of the Motional Narrowing Pedestal in the Wall-Coated Cell.....	21
3. SUMMARY.....	25
REFERENCES.....	27

Accession For	
NTIS GRA&I	<input checked="" type="checkbox"/>
DTIC TAB	<input type="checkbox"/>
Unannounced	<input type="checkbox"/>
Justification	
By _____	
Distribution/	
Availability Codes	
Dist	Avail and/or Special
A-1	



FIGURES

1. (a) Typical alkali ground state hyperfine transition lineshape in the presence of a few Torr of buffer gas. (b) Full Doppler profile of the alkali ground state hyperfine transition, observed in the absence of buffer gas..... 6
2. Linewidth of ^{87}Rb ground state hyperfine transition as a function of the ratio of a , the atom's mean free path, to λ , the transition wavelength..... 9
3. Hyperfine transition lineshape resulting from trajectory analysis of a ^{87}Rb atom in a wall-coated, bufferless cell..... 16
4. (a) Hyperfine lineshape for a ^{87}Rb atom in a 0.34-cm-radius, wall-coated, bufferless cell obtained from the trajectory calculation. (b) ^{87}Rb hyperfine lineshape after relationship between precollision velocities and postcollision velocities, found in the wall-coated, bufferless cell, has been ignored..... 17
5. Hyperfine lineshapes for ^{87}Rb atom in cells of varying radii..... 22

1. INTRODUCTION

The phenomenon of producing sub-Doppler spectral linewidths in atomic emissions by confining atoms with a buffer gas is well known. This line-narrowing effect was first analyzed by R. H. Dicke¹ and is typically termed Dicke narrowing. Dicke considered atoms confined by a nonperturbing buffer gas of sufficiently high pressure that the mean free path of the emitting atom was much less than the wavelength of the emitted radiation. Subsequent analyses²⁻⁶ have relieved this constraint and have produced a formalism that predicts a Doppler-broadened Gaussian lineshape in the limit of low buffer gas pressure and that reproduces Dicke's result: a narrowed Lorentzian lineshape in the limit of high buffer gas pressure. One of the most dramatic realizations of Dicke narrowing is observed in the magnetic dipole transitions of the hyperfine levels of alkali atoms. The ground state hyperfine transitions of ⁸⁷Rb and ¹³³Cs, at frequencies of 6.8 GHz and 9.2 GHz, respectively, have been extensively studied because of their applications in atomic frequency standards.⁷⁻¹⁰ In Fig. 1 we compare a typical lineshape that might be observed for the ground state hyperfine transition in ⁸⁷Rb in the presence of a few Torr of buffer, with a calculation of the full Doppler profile. Typically observed linewidths are about 300 Hz, and only a small fraction of that due to the residual Doppler contribution; the full Doppler width is computed to be around 10 kHz.

The lineshape derived by Dicke¹ is given by

$$\frac{I(\omega)}{I_0} = \frac{2\pi D/\lambda^2}{(\omega - \omega_0)^2 + (2\pi D/\lambda^2)^2} \quad (1.1)$$

where D is the diffusion constant of the atom through the particular buffer gas, and λ is the wavelength of the transition, $\lambda = c/2\pi\omega_0$. The full width at half intensity of the line is $4\pi D/\lambda^2$ (rad/s). For ⁸⁷Rb in a typical noble gas buffer, e.g., Kr, one computes the residual Doppler width, i.e., the Dicke-narrowed contribution, to be approximately 40 Hz/p , where p is the

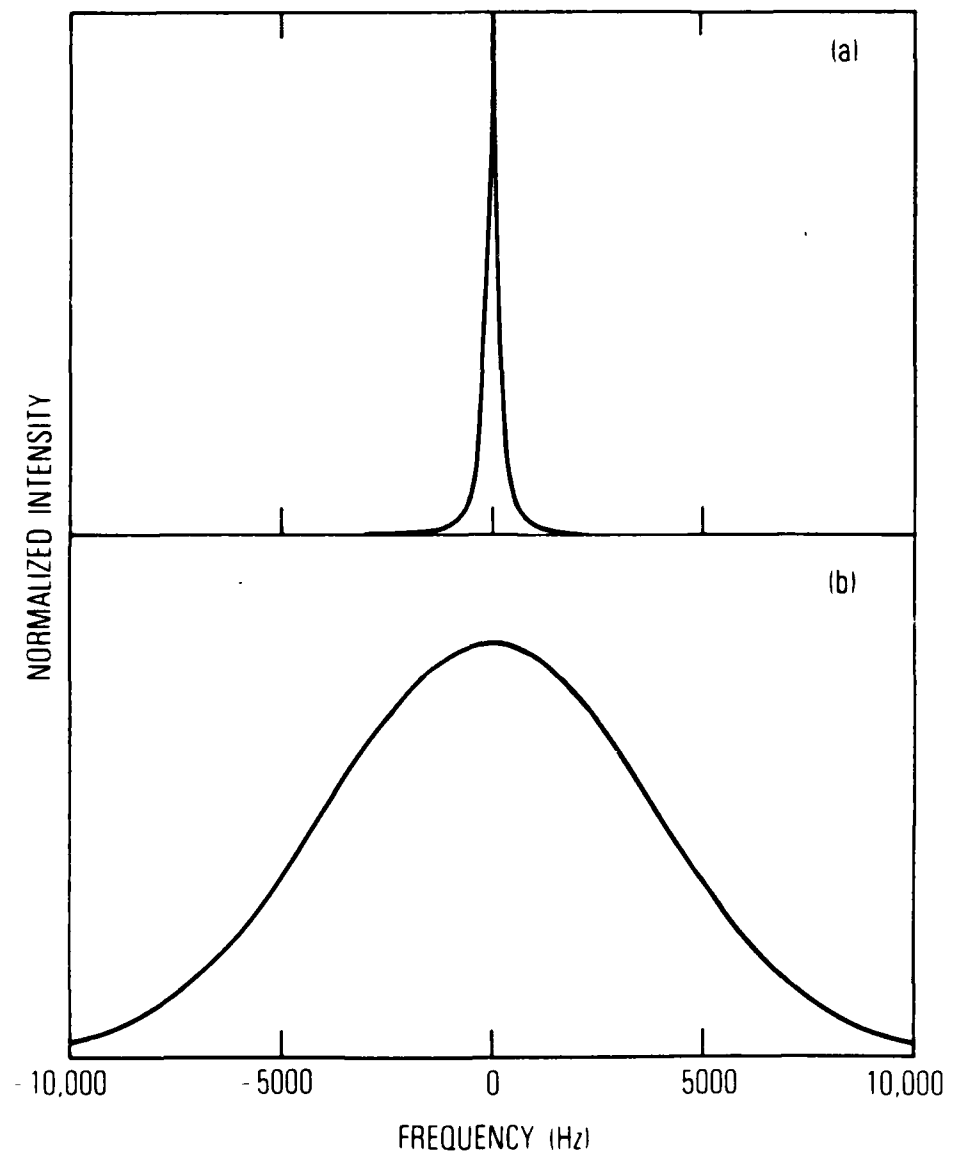


Figure 1. (a) Typical alkali ground state hyperfine transition lineshape in the presence of a few Torr of buffer gas. (b) Full Doppler profile of the alkali ground state hyperfine transition, observed in the absence of buffer gas.

pressure of the buffer in Torr. In a few Torr of buffer gas, then, the Dicke-narrowed contribution is only a very small fraction of the total linewidth. In the usual experiments, the major contributions to the linewidth arise from the effects of the optical pumping radiation, the microwave field, and magnetic field gradients and the like.

It is also well known that sub-Doppler linewidths can be obtained in absorption cells containing no buffer gases but having wall coatings, such as paraffin, to minimize the relaxation effects of wall collisions on the atomic spin orientation.¹¹⁻¹⁸ Microwave linewidths as narrow as 11 Hz have been observed in some of these experiments.¹⁸ The spectral narrowing of the rf or microwave lines in these bufferless, wall-coated cells has been explained by appealing to the example of an emitting atom confined to a one-dimensional box. In this model, an atom is confined to a box of dimension a , travels at constant velocity V , and is allowed only to rebound elastically, reversing direction upon a wall collision. It can be easily shown that for nonintegral values of a/λ the atom emits at both the normal unshifted frequency and the sideband frequencies determined by its velocity. For an ensemble of atoms with a Maxwell-Boltzmann velocity distribution confined to a one-dimensional box, one finds the lineshape to be composed of a central spike at the normal unshifted frequency, and a broad pedestal built up from the velocity-dependent sideband frequencies.

In reality, however, atoms confined to bufferless, wall-coated cells are not well described by the one-dimensional box model. All real cells are three dimensional. Simply generalizing the one-dimensional model to two dimensions changes the physical problem significantly. First, the distance that the atom may travel between collisions is no longer fixed; rather, it is distributed from zero to the diameter of the cell. Then, even if the atom is assumed to be emitted from the cell surface with a fixed speed S , a range of velocity components is still possible as the atom rebounds randomly within the cell. In two dimensions the well-defined sideband emission frequencies disappear. The range of velocities causes sideband frequency power to be spread over all frequencies between $\pm S_w / 2\pi c$. Averaging these lineshapes over a Maxwell-Boltzmann distribution results in a center peak resting on a non-Doppler

pedestal. Furthermore, purely elastic collisions with cell walls that allow atoms to bounce with no change in speed are not physically realistic. In fact, coated cell walls tend to be somewhat sticky. Atoms that collide with the coated wall stick for some period of time, between 10^{-11} and 10^{-10} s,¹³⁻¹⁴ and then are re-emitted at some random angle and random velocity governed by the respective angle and velocity distribution functions. Relaxing the condition of elastic collisions at the wall in the one-dimensional model also results in a sharp central spike resting on a clearly non-Doppler pedestal because, once again, each atom experiences a number of different velocities over its lifetime and thus would emit at numerous sideband frequencies so that the spectral power is spread out, leaving the greatest intensity at the normal unshifted frequency. For the various reasons outlined the "particle in a box" analysis of motional narrowing in bufferless, wall-coated cells is unsatisfying.

One aspect of Dicke's criterion for collisional lineshape narrowing¹ is that the emitting atom suffers collisions that do not perturb the atom's internal state. As indicated by Vanier *et al.*,¹⁰ collisions of emitting atoms with a buffer gas may be described in the same manner as collisions with a wall surface, both satisfying Dicke's criterion. Thus an atom undergoing hyperfine transitions should not really "know" if it is confined by a buffer gas or a wall, and consequently, one should not need two apparently distinct formalisms, buffer gas and particle in a box, to describe spectral line narrowing under collisional confinement. However, a naive application of the line-narrowing formalism to the bufferless, wall-coated cell completely fails. In Fig. 2 we plot the full width at half intensity of the residual Doppler contribution to the ⁸⁷Rb microwave lineshape at 6.8 GHz, as predicted by the complete line-narrowing formalisms, versus the dimensionless parameter a/λ , where a is the mean free path of the atoms. The area to the left of the dashed line in the figure indicates the region of applicability of Dicke's result. To the right of the dashed line, the linewidth is seen to smoothly go to the full Doppler width, as expected. In addition, we have also plotted in

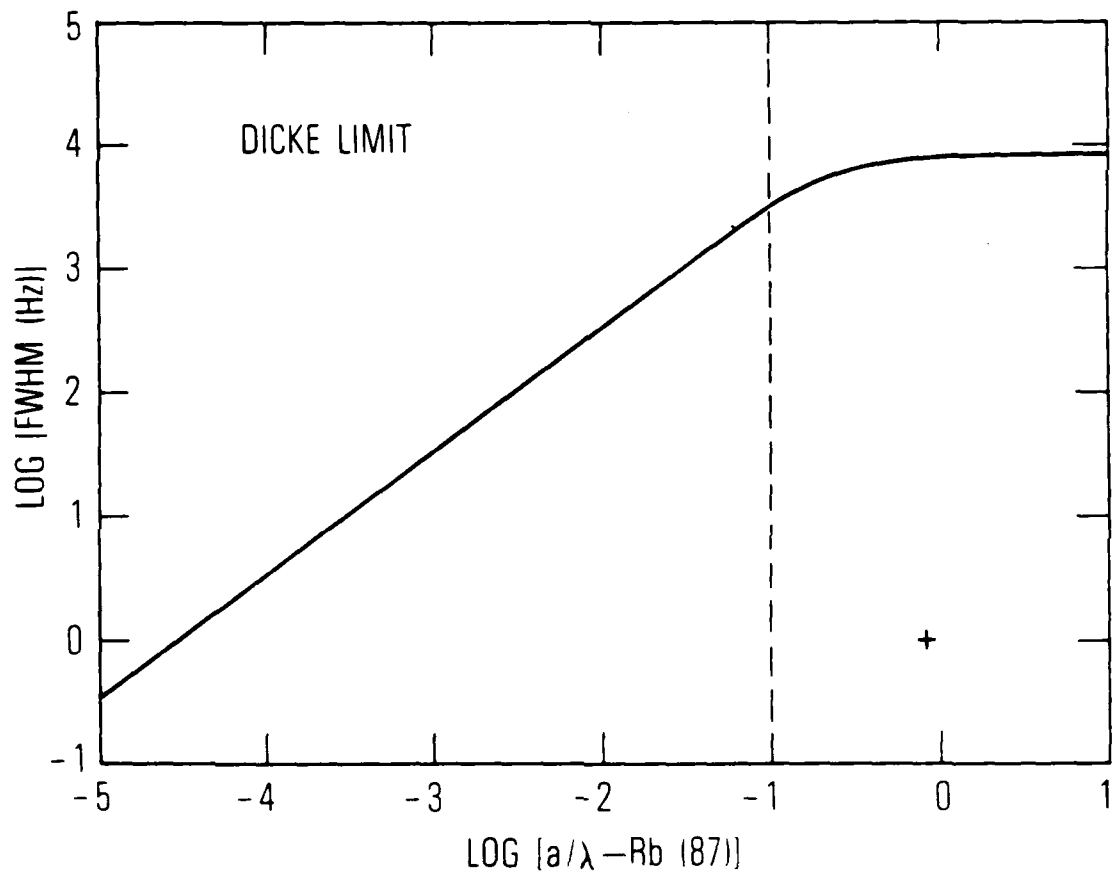


Figure 2. Linewidth of ^{87}Rb ground state hyperfine transition as a function of the ratio of a , the atom's mean free path, to λ , the transition wavelength. Linewidths were calculated according to Galatry.² The dashed line represents the limit of validity of Dicke's original analysis.¹ The "+" symbol corresponds to the estimate of the residual Doppler contribution to the measured linewidth in Ref. 12.

Fig. 2 the estimate of the residual Doppler contribution to the linewidth observed by Robinson and Johnson,¹⁸ denoted by the symbol "+". In this particular case we took the mean free path of the Rb atoms to be the radius of the absorption cell. It is quite apparent that the standard formulations of line narrowing fail dramatically in this situation.

We have investigated the line-narrowing phenomenon in a bufferless, wall-coated absorption cell following the same formalisms developed for the buffered cell. Particle trajectories within the absorption cell were generated using Monte Carlo techniques. This method of analyzing atomic motion in a spherical cell has been applied previously to motional narrowing of Zeeman lineshapes in the presence of an inhomogeneous magnetic field.^{19,20} This form of analysis is particularly appropriate for hyperfine transitions, because wall coatings exist that minimize hyperfine state changes during the wall collision. We have found that, although the trajectories followed by the atom over its hyperfine state lifetime have a statistical nature because atoms striking the coated wall are adsorbed for a finite time and then re-emitted randomly, there still is a very high probability that the Doppler shifts before and after a particular wall collision are of opposite sign. This leads to an effective cancellation of Doppler-shift effects. The resulting lineshape displays a sharp central spike resting on a clearly non-Gaussian pedestal. Additionally, analysis of the atomic trajectories in a wall-coated cell demonstrates a correlation between postcollision velocities and inter-collision times. While not of great significance in these cells, a similar correlation, albeit a much weaker one, exists in the buffered cell. This correlation, which has been completely neglected in previous analyses of the line-narrowing phenomenon, will lead to additional narrowing of the residual Doppler contribution beyond that given in the standard analyses. A major value of our new analysis is that spectral line narrowing due to confining collisions can be explained by a single formalism no matter what the origin of the confining collisions.

2. ANALYSIS AND RESULTS

An effective method of analyzing certain aspects of radiation problems, as pointed out by Weisskopf,²¹ is to treat each radiating atom as a classical oscillator. This technique has been exploited in previous analyses of line narrowing for an atom surrounded by a buffer gas.^{2,4} The displacement of the oscillator, $x(t)$, is given by

$$x(t) = A \cos[\omega_0 t + \frac{\omega_0}{c} \int_0^t v_x(\tau) d\tau] \quad (2.1)$$

with ω_0 the atomic transition frequency, v_x the velocity component leading to the Doppler shift, c the speed of light, and A a constant. For the time $T(i)$ between the $(i-1)$ th and i th collisions with the buffer gas atoms, the radiating atom has a fixed velocity $v_x(i)$. This allows Eq. (2.1) to be rewritten as

$$x(t) = A \cos [\omega_0 t + \frac{\omega_0}{c} \sum_{i=1}^N v_x(i) T(i)] \quad (2.2)$$

with N being the number of collisions in time t .

Typically, the postcollision velocities and intercollision times are treated as independent, stationary, random variables. The autocorrelation function of the oscillator, $F(\tau)$, is given by²²

$$F(\tau) = \langle x(0) \cdot x(\tau) \rangle \quad (2.3)$$

where the brackets indicate stochastic averaging over the random variables v_x and T . To perform the averaging requires the probability density functions for the random variables. For the radiating atom surrounded by a buffer gas the postcollision velocities are distributed according to the Maxwell-Boltzmann distribution; the intercollision times are assumed to be distributed according to a simple Poisson distribution.⁴ In this model, the velocity, and hence the Doppler shift after a collision, is assumed to be completely independent of those prior to the collision. The Fourier transform of the

autocorrelation function is the oscillator's power spectral density or, in this case, would be more appropriately termed the transition lineshape. Line-widths obtained using this procedure yield the solid curve plotted on Fig. 2.

2.1 ANALYSIS OF MOTIONAL NARROWING IN THE WALL-COATED CELL

It has been shown that the naive application of the results of the standard buffer gas analysis to motional narrowing in the wall-coated cell does not yield the correct linewidth. Carrying out a more detailed analysis of the wall-coated cell case within the stochastic averaging framework is not straightforward, because (1) while the postcollision velocities will undoubtedly be distributed in a Maxwell-Boltzmann form, it is not obvious that the intercollision times are still distributed according to a Poisson distribution, and (2) the assumption that there is no relation between the velocity and Doppler shift before and after a collision is no longer even approximately correct. In a coated cell there is a high probability that the velocities before and after a collision will have opposite signs and their Doppler shifts will tend to cancel. In effect, a Markoffian relation exists between the velocities before and after a collision. Aspects of the effects of similar relationships have been discussed by Anderson²³ and Kubo²⁴ with regard to motional narrowing in nuclear magnetic resonance (NMR) spectra. However, attempting to apply their analyses to this problem is quite difficult.

An alternative to these standard stochastic analyses is to explicitly obtain $x(t)$ as a function of time and then perform its Fourier analysis. To carry this out, a series of $V_x(i)$'s and $T(i)$'s as would be observed in a wall-coated cell must be generated. This has been done by calculating the classical trajectories of a particle in the wall-coated cell. A similar method of analysis was applied by Watanabe *et al.*¹⁹ in their study of the motional narrowing of Zeeman lineshapes for atoms in inhomogeneous magnetic fields. They found this Monte Carlo analysis to be quite effective for their problem.

It is well known that, in collisions between alkali atoms and cell walls coated with materials like paraffin, the colliding atoms are physically adsorbed and then re-emitted.^{13,14} The direction of re-emission is

characterized by two angles, θ and ϕ . Angle θ ranges from $-\pi/2$ to $\pi/2$ with respect to the direction normal to the cell wall at the point the particle has impacted. Angle ϕ is the azimuthal angle about the normal direction and varies from 0 to 2π . The angle θ has been found to be cosine distributed;^{*,25} ϕ is uniformly distributed throughout its range. The $\cos(\theta)$ dependence results in equal probabilities for traveling from the initial surface point to any other point on the sphere surface. Consequently, given the initial point, the next impact may be determined by randomly selecting a point on the surface of the sphere. The emission speed S was assumed to satisfy the Maxwell-Boltzmann speed distribution. Generation of a random variable satisfying this distribution was performed using standard techniques.^{26,27} Once a particular S and the next impact point are selected, it is possible to determine the intercollision time and the component of velocity in the direction of the detector, $V_x(i)$, that leads to the Doppler shift. Repeating this procedure enables generation of a full particle trajectory.

To account for the finite coherence lifetime t_0 of the radiating atom, Eq. (2.2) assumes the form

$$x(t) = \begin{cases} A \cos [\omega_0 t + \frac{\omega_0}{c} \sum_{i=1}^N V_x(i) T(i)] & t < t_0 \\ 0 & t > t_0 \end{cases} \quad (2.4)$$

^{*}Recent experimental measurements performed by L. R. Martin and C. M. Kahla of The Aerospace Corporation show that Cs particles recoiling from a paraffin surface satisfy a $\cos(\theta)$ distribution. A similar emission distribution should be satisfied by Rb atoms recoiling from a paraffin coating in the standard wall-coated cell.

where the $V_x(i)$'s and $T(i)$'s are from the trajectory calculation, Eq. (2.2). Rather than calculating the autocorrelation function of $x(t)$ and then obtaining the lineshape from its Fourier transform, we performed the direct Fourier analysis of $x(t)$. The lineshape $G(\omega)$ is related directly to $x(t)$ in Eq. (2.5):²⁸

$$G(\omega) = \left| \int_{-\infty}^{+\infty} e^{-i\omega t} x(t) dt \right|^2 \quad (2.5)$$

The Fourier transform of $x(t)$ was computed numerically and was facilitated by noting that between collisions the radiation from the atom appears to have a fixed frequency and that the frequency changes discretely upon each collision. Equation (2.5) can then be broken into a sum of integrals, one for each intercollision period, with each of the integrals capable of being evaluated analytically.

Strictly speaking one should explicitly take into account the fact that t_0 represents an average lifetime of the atom and weight the collisional effects over the atom's lifetime using an exponential function. Because the average lifetime is so much larger than the average intercollision time in the systems of interest, only a very few atoms do not participate in the collisional averaging. As will be shown, collisional narrowing in these systems is extremely effective, and thus (for clarity) we decided to consider only an average atomic state lifetime, knowing that under the specified conditions the error will be negligible. However, in a more general situation in which a substantial fraction of the atoms have relatively few collisions over their lifetimes, a properly weighted lifetime function would have to be incorporated into Eq. (2.4) and appropriate averaging performed. One further computational aspect should also be discussed. Oscillator trajectory $x(t)$ is specified by a trajectory lasting a period t_0 . In principle, an infinite number of different trajectories, each lasting t_0 , can be generated. Each trajectory will yield a different $x(t)$ with a slightly different $G(\omega)$. To obtain the desired accuracy in the calculated lineshapes, several hundred trajectories were averaged together, corresponding to approximately 100,000 wall collisions for each lineshape.

Application of this computational procedure to ^{87}Rb at 25°C in a wall-coated spherical cell with a radius of 3.4 cm yields the lineshape shown in Fig. 3. The linewidth is approximately 10 Hz, indicating that in the wall-coated cell Dicke narrowing effectively removes all Doppler broadening and yields the linewidth specified by the radiating atom's coherence lifetime in the cell, approximately 0.1 s. This result is in agreement with the measurements of Robinson and Johnson,¹⁸ in which no residual Doppler broadening was observed. The small oscillations in the figure are due to the computational model, in which the atomic radiation is stopped abruptly at t_0 . Averaging lineshapes of this type, generated from an exponential distribution of radioactive lifetimes, would yield the expected Lorentzian lineshape. Additionally the central peak is found to be resting on a broad, non-Gaussian, pedestal with a width of approximately two-thirds that of the calculated Doppler width. Published experimental observations of pedestals are limited; however, Robinson and Johnson¹⁸ report a Gaussian pedestal, whose width equalled the full Doppler linewidth. Although the trajectory formalism that we have described provides an excellent model for linewidth narrowing, there is at present some difficulty in reproducing the pedestal portion of the line as experimentally observed. We discuss the implications of this problem in Section 2.3.

The extremely efficient Dicke narrowing yielding the central peak found in the wall-coated, bufferless cell is due primarily to the high probability that the velocity after a collision will have the opposite sign to that prior to the collision, thereby cancelling the Doppler shifts. The significance of this relationship between the pre- and postcollision velocities may be readily demonstrated by repeating the trajectory calculation. However, this time, upon each collision, the position of the particles is randomized over cell surface. While each trajectory is still subject to the spatial constraints of the cell and the cosine emission distribution, any "memory" of a prior velocity is removed.

Figure 4a depicts the lineshape for a particle in a 0.34-cm-radius, wall-coated, bufferless cell obtained from the standard trajectory calculation. Beneath it, Fig. 4b indicates the lineshape resulting from the modified

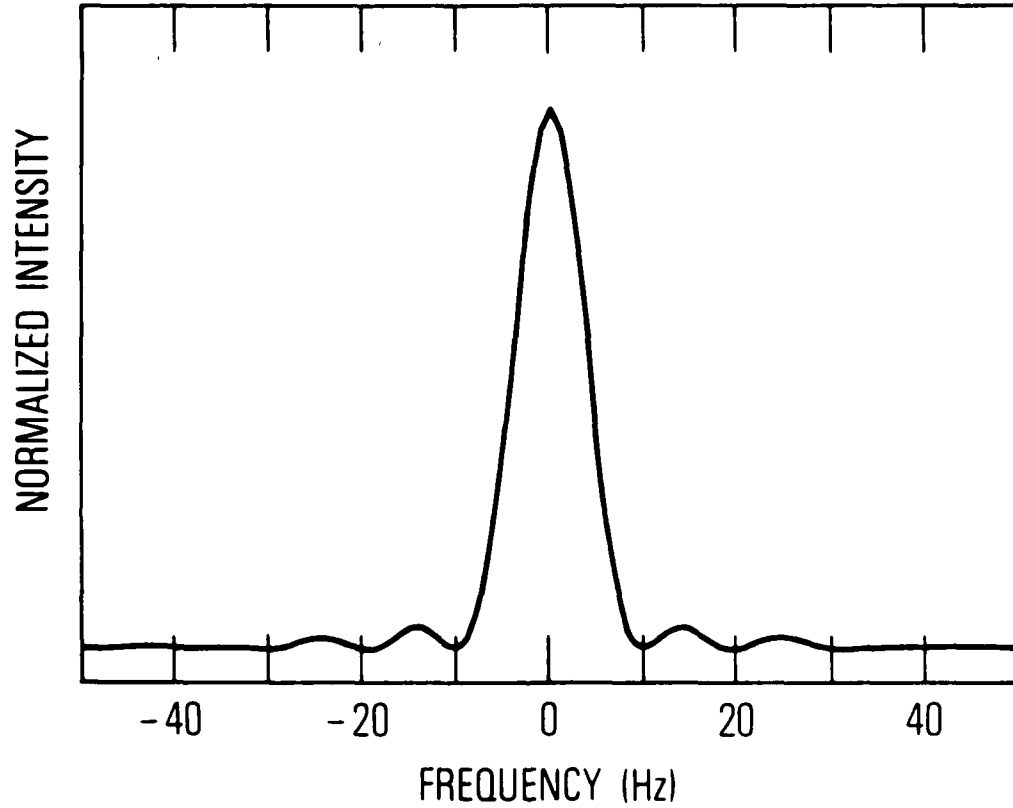


Figure 3. Hyperfine transition lineshape resulting from trajectory analysis of a ^{87}Rb atom in a wall-coated, bufferless cell. The cell radius is 3.4 cm, and the temperature is 25°C.

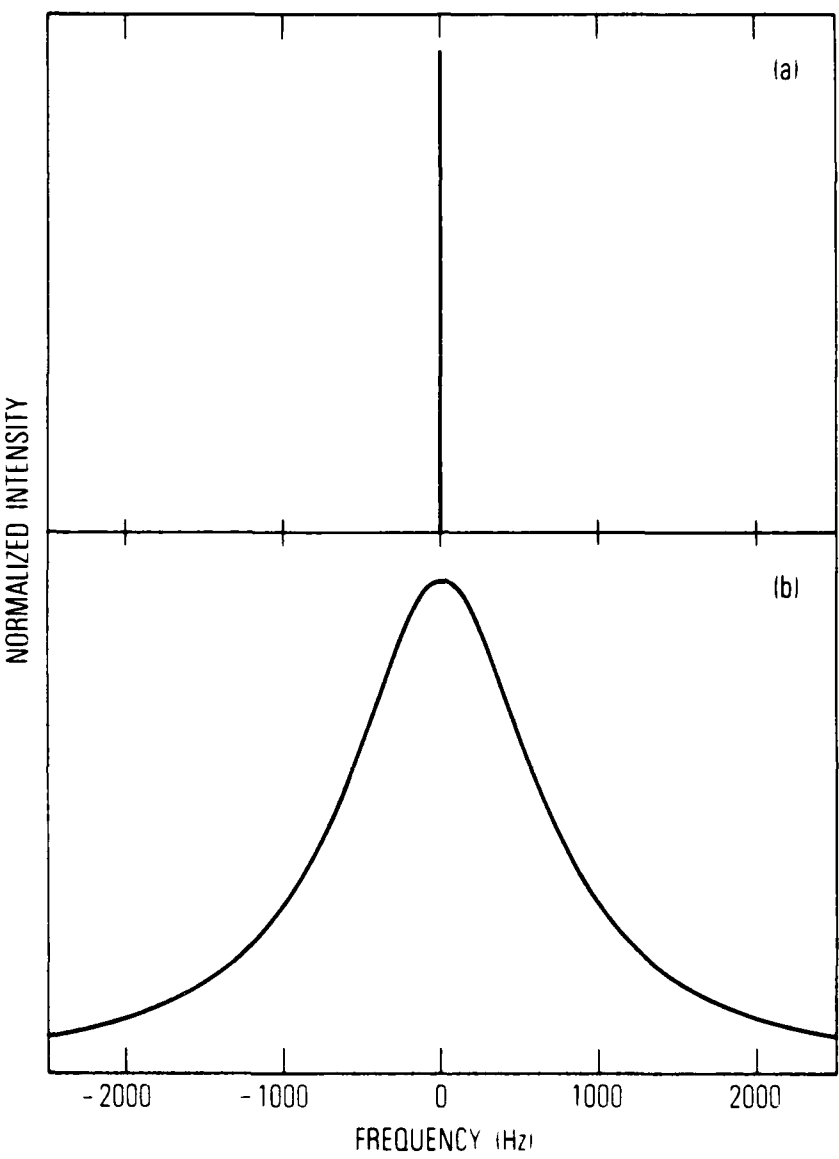


Figure 4. (a) Hyperfine lineshape for a ^{87}Rb atom in a 0.34-cm-radius, wall-coated, bufferless cell obtained from the trajectory calculation. The linewidth is 10 Hz. (b) ^{87}Rb hyperfine lineshape after relationship between precollision velocities and postcollision velocities, found in the wall-coated, bufferless cell, has been ignored. The linewidth is approximately 1400 Hz.

trajectory calculation just described. The 0.34-cm radius was chosen for clarity of example such that the uncorrelated linewidth would still be well below the full Doppler width. The linewidth in Fig. 4b is approximately 1400 Hz, over two orders of magnitude larger than the 10-Hz linewidth of Fig. 4a. The linewidth displayed in Fig. 4b is essentially the same as predicted by the standard statistical analyses of Dicke narrowing in a buffer gas. Subtle differences between the lineshape displayed in Fig. 4b and that given by the standard analyses are due to the non-Poisson intercollision time distribution in the wall-coated cell and thus an exact comparison with Fig. 2 is not appropriate. This calculation clearly verifies that it is the relationship between the precollision and postcollision velocities that leads to the extremely effective narrowing in a wall-coated, bufferless cell.

2.2 ANALYSIS OF MOTIONAL NARROWING IN THE BUFFER-GAS CASE

Examination of the trajectories of atoms in the wall-coated, bufferless cell shows that there is a correlation between the postcollision velocity of an atom and the intercollision time. Faster-moving atoms typically have shorter intercollision times. For the bufferless cell, the trajectory analysis includes these effects. Any similar correlation in the buffer gas cell has typically not been taken into account in the standard Dicke calculations. The standard statistical analysis of motional narrowing for a particle surrounded by a buffer gas assumes that the postcollision velocities and intercollision times are completely independent. While this is a fairly good assumption it is not rigorously correct. Some correlation exists even in the buffer-gas case, albeit not nearly as strong as that in the wall-coated cell. Clearly, the velocity of the radiating atom will affect to some extent the intercollision time.

Typically, intercollision times are assumed to obey the simple Poisson distribution, and the most probable intercollision time is the inverse of the average collision frequency.²⁹ Most probable intercollision time τ_p does not depend on the precise speed of the radiating atom after each collision but is a function of the speed of the radiating atom. The relation between the most probable collision time of a radiating atom with a precise speed S surrounded

by a buffer gas of mass m , at temperature T , and with a number density N is given by³⁰

$$(\tau_p)^{-1} = N \pi \sigma^2 (\pi \beta)^{-1/2} (\beta^{1/2} s)^{-1} \psi(\beta^{1/2} s) \quad (2.6)$$

with

$$\psi(x) = x e^{-x^2} + (2x^2 + 1) \int_0^x e^{-y^2} dy \quad (2.7)$$

$$\beta = \frac{m}{2kT} \quad (2.8)$$

and k the Boltzmann constant.

To analyze the effects of correlation in the buffer-gas case, $x(t)$ as specified in Eq. (2.4) is generated. After each collision a random speed $s(i)$ is generated by taking the magnitude of a velocity vector whose three components were randomly selected from independent Maxwell-Boltzmann velocity distributions. This clearly is a simplistic model, considering that the postcollision speed may be strongly related to the precollision speed. However, it is felt to be adequate, because our primary interest is in the relationship between postcollision speed and intercollision time--two quantities typically taken to be uncorrelated. Velocity component $v_x(i)$ generates the Doppler shift after the i th collision. The intercollision times are chosen as follows. Given the postcollision speed, a most probable intercollision time $\tau_p(i)$ is calculated using Eqs. (2.6) through (2.8). This time is then used as the most probable intercollision time for the Poisson distribution from which a particular intercollision time $T(i)$ is chosen. Since the postcollision speed changes after each collision, the most probable intercollision time, a function of that speed, also changes after each collision. Consequently, after each collision, $T(i)$ is chosen from a different Poisson distribution. In this way the mild correlation between intercollision times and postcollision speeds found even in the buffer-gas case is rigorously taken into account. Once the postcollision speeds, velocities, and intercollision times are specified, $x(t)$ is defined and may be

Fourier-analyzed, as was the bufferless, wall-coated cell, to yield the lineshape.

The calculation was performed for a system in which the correlation should be enhanced. Hydrogen, with a hyperfine frequency of 1.42 GHz, was chosen as the emitting species; Kr was used as the buffer species. Because Kr is larger in mass than H, its buffer atoms appear almost motionless to the rapidly moving H atoms. A system temperature of 25°C was used, and the radiative lifetime of the H atom was taken to be 0.025 s. The ratio of the mean free path to the emitted wavelength was set at 0.01, placing the calculation within the standard Dicke regime. The calculated lineshape is Lorentzian, with a linewidth of approximately 220 Hz. Since the linewidth is well above that specified by the atom's radiative lifetime, there is no need to increase the radiative lifetime employed in the calculation.

The buffer-gas calculation was repeated, but instead of the velocity-dependent intercollision times based on Eqs. (2.6) through (2.8), speed-independent intercollision times were used. These times were chosen randomly from a Poisson distribution whose most probable collision time τ'_p was given by:²⁹

$$(\tau'_p)^{-1} = \pi \sigma^2 N v_m \quad (2.9)$$

with

$$\sim v_m = \left(\frac{2 k T}{M^*} \right)^{1/2} \quad (2.10)$$

and M^* the H-Kr reduced mass. This calculation also resulted in a Lorentzian lineshape; however, the linewidth was nearly 370 Hz. The inclusion of the correlation effects yields a linewidth reduced by 40% from the uncorrelated linewidth. We find that even in the buffer-gas case the effects of the correlation between intercollision times and postcollision velocities must be taken into account.

2.3 DISCUSSION OF THE MOTIONAL NARROWING PEDESTAL IN THE WALL-COATED CELL

As indicated in Section 2.1, the trajectory analysis we described is in excellent agreement with the observations of spectral line narrowing, but seems to have some difficulty in exactly reproducing the experimentally measured pedestals on which the narrowed portion of the spectral line is found. To investigate the computationally generated pedestal, lineshapes were calculated for a number of cells of radii ranging from 1.5 to 40 cm. In Fig. 5, several of these curves are presented. As would be expected from the one-dimensional analysis, with increasing cell radius the height of the pedestal with respect to that of the central peak becomes larger. In each case, though, the pedestal remains non-Gaussian with a width of approximately 6 kHz.

To ensure that this nonagreement in the pedestal region of the spectral lineshape was not a computational artifact, the algorithm was subjected to a series of tests. The linewidth of the central spike is exactly what is expected from the simple Fourier analysis of a sinusoidal wavetrain persisting for the t_0 employed in the calculation. The effects on the central spike of the frequency changes due to velocity-changing collisions are completely removed. If a single fixed atomic velocity is supplied to the Fourier transform algorithm, spectral intensity is generated at the correct Doppler-shifted frequency. As another test, rather than generating velocities and intercollision times from atomic trajectories within the wall-coated cell, these quantities are chosen to be appropriate for a Rb atom surrounded by a buffer gas, as described in Section 2.2. The resulting lineshapes match exactly the results of the standard statistical analyses of Dicke narrowing. The lineshapes change smoothly from narrow Lorentzians at small mean free paths to full Doppler lineshapes at large mean free paths. In light of these tests, we feel that the algorithm is correctly calculating the motionally narrowed lineshape appropriate to the physical model we have described.

In modeling the signals of interest, several simplifying approximations have also been analyzed. First, the radiating atoms are known to stick to the cell surface for times on the order of 10^{-11} to 10^{-10} s, during which the radiated frequency is significantly perturbed by interactions with the cell

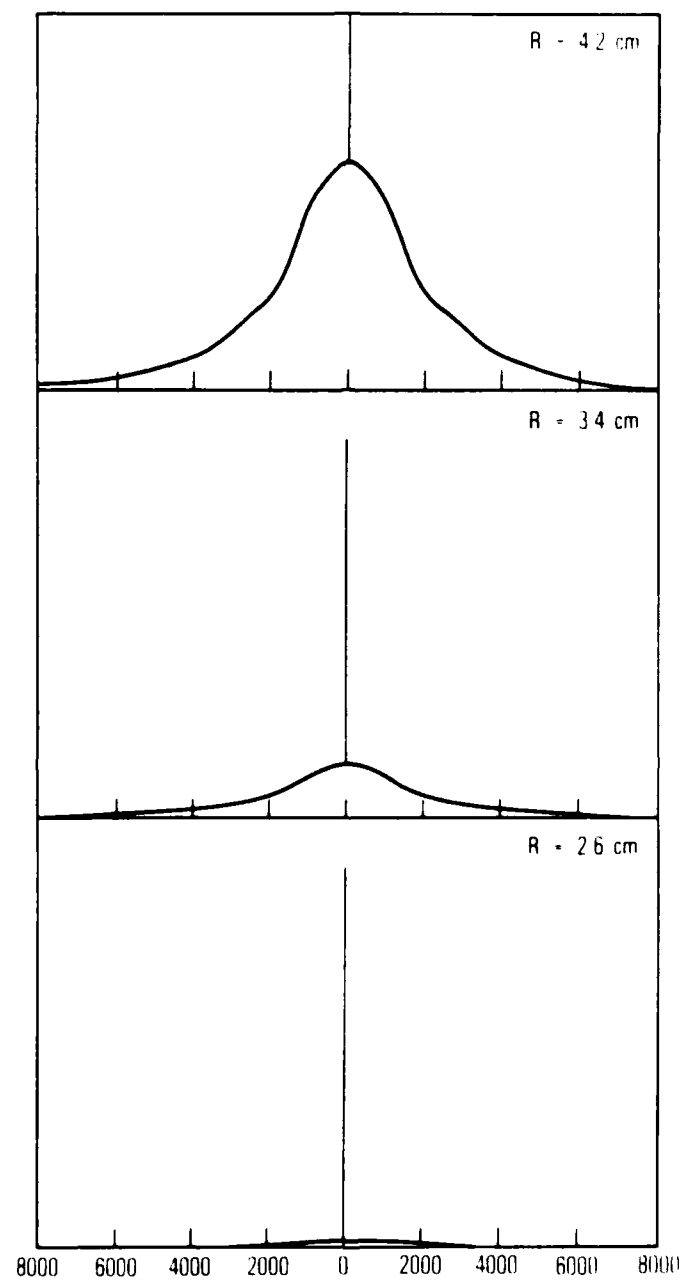


Figure 5. Hyperfine lineshapes for ^{87}Rb atom in cells of varying radii.

walls. From the results of Vanier *et al.*¹⁰ the magnitude of this shift for atoms residing on the surface for 10^{-10} s is approximately 64 MHz. To observe the effects of this process, calculations were performed in which, between each atomic trajectory, the atom was assumed to reside on the cell surface for 10^{-10} s and radiate at the shifted frequency. Including this wall sticking did not modify the calculated pedestals.

An additional difference between the calculational model and physical reality is associated with how the atom's loss of coherence is treated. The coherence time specifies the width of the central peak. In our calculation the atom is allowed to radiate within the cell for the coherence time t_0 , and all coherence is lost instantaneously at t_0 . In reality, coherence is lost "gradually" from small random changes in the phase of the radiation upon each wall collision. To explicitly include this gradual loss of coherence, an additional random variable $\eta(\tau)$ was included within the argument of the cosine in Eq. (2.1) and was assumed to be a Gaussian random variable whose value changed upon each collision with the wall. With the inclusion of $\eta(\tau)$, the central peak's linewidth could be controlled by the magnitude of $\eta(\tau)$'s variations rather than by specifying a somewhat artificial t_0 . However, treating coherence loss in this manner does not change the pedestal.

Finally, we have investigated the effects of nonuniform microwave intensity across the absorption cell as is the normal experimental condition when horns are used as part of the microwave source. Although the analysis was developed for a uniform strength, it is possible to treat the variable field strength in a straightforward manner. As an extreme case we considered a point source located several centimeters from the storage. The resulting A-factor in Eq. (2.1) is now position dependent. While Eq. (2.5) may still be broken into a sum of integrals, one for each intercollision period, the integration of each of these integrals was carried out numerically. Even for the extreme case of a point microwave source, the resulting pedestals were identical to those calculated previously, indicating that an incomplete description of the microwave field strength variation within the storage cell is most likely not the source of the unexpected pedestal.

The pedestals obtained computationally are not well described by either Gaussian or Lorentzian lineshapes. They are well fit, though, by the sum of two Gaussians of approximately equal heights but with differing widths. One Gaussian has a width approximately equal to the expected Doppler width of 9 kHz; the other has a width of about 4 kHz. Only when the cell radius is significantly increased do the relative heights of the two Gaussians change. For example, when the cell radius is set at 40 cm the narrow Gaussian's height is only 25% that of the broader Gaussian.

An interesting observation concerning the pedestal shape was made. If the atom's emission time and the storage cell radius are properly chosen, no collision with the wall will occur during the emission period. Averaging a large number of these collisionless trajectories yields a pedestal of standard Doppler lineshape. However, once the trajectories are selected such that, on the average, a single wall collision occurs during each trajectory, the pedestal reverts to the double Gaussian form. The fact that the effects of collisions in the spherical cell become apparent after a single collision is consistent with the findings of Sykes.²⁰ When studying motional narrowing of Zeeman resonance lineshapes in inhomogeneous magnetic fields, he found that considering only the initial motions of atoms within spherical cells up to their second wall collisions defined the lineshapes quite adequately.

At this point we are unable to explain the apparent discrepancy between the calculated pedestal and the experimentally observed pedestal. The calculations accurately calculate the Dicke-narrowed lineshape. The fact that there are significant differences between the calculated and observed pedestals may mean that the pedestal region of the spectral lineshape is extremely sensitive to the particular experimental conditions. There is a paucity of detailed experimental measurements of the spectral lineshape's pedestal region, since the narrowed portion of the lineshape has always been of more interest from the aspects of both its fundamental physics and its application to various devices such as atomic frequency standards. Further experimental investigations into the pedestal region of these narrowed spectral lineshapes could now prove extremely beneficial in improving our understanding of atom-atom and atom-wall collisions and spectral line-narrowing processes.

3. SUMMARY

It has been shown that a single formalism can be used to describe Dicke narrowing, collisionally induced motional narrowing. The extreme narrowing observed in the wall-coated, bufferless cell results from the high probability that the precollision and postcollision velocities will be of opposite sign, thereby cancelling Doppler shifts. The pedestals observed beneath the narrow central spike are non-Doppler, more accurately described by the sum of two Gaussians, one with the Doppler width and a second with a width of approximately half the Doppler width. The calculated form of the pedestal is not in agreement with the limited available experimental data that show a Doppler pedestal. For atoms confined in a buffer gas, the effect of the mild correlation between the postcollision velocities and intercollision times has been analyzed. Including this mild correlation results in a somewhat narrower line than is predicted by the standard analyses of Dicke narrowing, which neglect its effect.

REFERENCES

1. R. H. Dicke, Phys. Rev. 89, 472 (1953).
2. L. Galatry, Phys. Rev. 122, 1218 (1960).
3. S. G. Rautian and I. I. Sobel'man, Soviet Phys. Usp. 9, 701 (1967).
4. J. I. Gersten and H. M. Foley, J. Opt. Soc. Am. 58, 933 (1968).
5. D. R. A. McMahon, Aust. J. Phys. 34, 639 (1981).
6. M. N. Neuman and G. C. Tabisz, J. Quant. Spectrosc. Radiat. Transfer 29, 267 (1983).
7. M. Arditi and T. R. Carver, Phys. Rev. 124, 800 (1961).
8. M. Arditi and T. R. Carver, Phys. Rev. 126, A643 (1964).
9. C. W. Beer and R. A. Bernheim, Phys. Rev. A13, 1052 (1974).
10. J. Vanier, D. H. Nguyen, G. Busca, and M. Tetu, Can. J. Phys. 57, 1380 (1979).
11. H. M. Goldenberg, D. Kleppner and N. F. Ramsey, Phys. Rev. 123, 530 (1961).
12. M. A. Bouchiat, J. Phys. Paris 24, 379 (1963).
13. R. B. Brewer, J. Chem. Phys. 38, 3015 (1963).
14. M. A. Bouchiat and J. Brossel, Phys. Rev. 147, 41 (1966).
15. C. W. White, W. M. Hughes, G. S. Hayne, and H. G. Robinson, Phys. Rev. 174, 23 (1968).
16. J. Vanier, J. F. Simard, and J. S. Boulanger, Phys. Rev. A 9, 1031 (1974).
17. A. Risely, S. Jarvis, and J. Vanier, J. Appl. Phys. 51, 4571 (1980).
18. H. G. Robinson and C. E. Johnson, Appl. Phys. Lett. 40, 771 (1982).
19. S. F. Watanabe, G. S. Haynes, and H. G. Robinson, J. Phys. B: Atom. Molec. Phys. 10, 941 (1977).
20. J. Sykes, J. Phys. B: Atom. Molec. Phys. 10, 1151 (1977).
21. V. F. Weisskopf, Rev. Mod. Phys. 21, 305 (1949).

22. W. B. Davenport and W. L. Root, An Introduction to the Theory of Random Signals and Noise, McGraw-Hill, New York (1958).
23. P. W. Anderson, J. Phys. Soc. Jpn. 9, 316 (1954).
24. R. Kubo, Fluctuation, Relaxation and Resonance in Magnetic Systems, ed. D. ter Haar, Oliver and Boyd, Edinburgh (1962).
25. E. C. Cashwell and C. J. Everett, A Practical Manual on the Monte Carlo Method for Random Walk Problems Pergamon, New York (1959), p. 19.
26. J. M. Hammersley and D. C. Handscomb, Monte Carlo Methods, Methuen and Co., London (1964), p. 39.
27. H. Kahn, Applications of Monte Carlo Rand, Santa Monica, CA (1956).
28. R. B. Blackman and J. W. Tukey, The Measurement of Power Spectra, Dover, New York (1958).
29. R. D. Present, Kinetic Theory of Gases, McGraw-Hill, New York (1958), p. 30.
30. R. J. C. Brown, Can. J. Chem. 44, 1421 (1966).

LABORATORY OPERATIONS

The Aerospace Corporation functions as an "architect-engineer" for national security projects, specializing in advanced military space systems. Providing research support, the corporation's Laboratory Operations conducts experimental and theoretical investigations that focus on the application of scientific and technical advances to such systems. Vital to the success of these investigations is the technical staff's wide-ranging expertise and its ability to stay current with new developments. This expertise is enhanced by a research program aimed at dealing with the many problems associated with rapidly evolving space systems. Contributing their capabilities to the research effort are these individual laboratories:

Aerophysics Laboratory: Launch vehicle and reentry fluid mechanics, heat transfer and flight dynamics; chemical and electric propulsion, propellant chemistry, chemical dynamics, environmental chemistry, trace detection; spacecraft structural mechanics, contamination, thermal and structural control; high temperature thermomechanics, gas kinetics and radiation; cw and pulsed chemical and excimer laser development including chemical kinetics, spectroscopy, optical resonators, beam control, atmospheric propagation, laser effects and countermeasures.

Chemistry and Physics Laboratory: Atmospheric chemical reactions, atmospheric optics, light scattering, state-specific chemical reactions and radiative signatures of missile plumes, sensor out-of-field-of-view rejection, applied laser spectroscopy, laser chemistry, laser optoelectronics, solar cell physics, battery electrochemistry, space vacuum and radiation effects on materials, lubrication and surface phenomena, thermionic emission, photo-sensitive materials and detectors, atomic frequency standards, and environmental chemistry.

Computer Science Laboratory: Program verification, program translation, performance-sensitive system design, distributed architectures for spaceborne computers, fault-tolerant computer systems, artificial intelligence, micro-electronics applications, communication protocols, and computer security.

Electronics Research Laboratory: Microelectronics, solid-state device physics, compound semiconductors, radiation hardening; electro-optics, quantum electronics, solid-state lasers, optical propagation and communications; microwave semiconductor devices, microwave/millimeter wave measurements, diagnostics and radiometry, microwave/millimeter wave thermionic devices; atomic time and frequency standards; antennas, rf systems, electromagnetic propagation phenomena, space communication systems.

Materials Sciences Laboratory: Development of new materials: metals, alloys, ceramics, polymers and their composites, and new forms of carbon; non-destructive evaluation, component failure analysis and reliability; fracture mechanics and stress corrosion; analysis and evaluation of materials at cryogenic and elevated temperatures as well as in space and enemy-induced environments.

Space Sciences Laboratory: Magnetospheric, auroral and cosmic ray physics, wave-particle interactions, magnetospheric plasma waves; atmospheric and ionospheric physics, density and composition of the upper atmosphere, remote sensing using atmospheric radiation; solar physics, infrared astronomy, infrared signature analysis; effects of solar activity, magnetic storms and nuclear explosions on the earth's atmosphere, ionosphere and magnetosphere; effects of electromagnetic and particulate radiations on space systems; space instrumentation.

...

ENVO

DTIC

6 - 86